Chapter 11

OPTIONS

Contents

11.1 Introduction

Up to this point, this report has discussed the design of a muon collider with:

1. beam energies of 2 + 2 TeV
2. operating at its maximum energy
3. with a fixed rms energy spread of 0.12%

4. with no attention to maximizing polarization

In this section we discuss modifications to enhance the muon polarization's, operating parameters with very small momentum spreads, operations at energies other than the maximum for which a machine is designed, and designs of machines for different maximum energies. In particular we will give parameters of machines with center of mass energy of 0.5 TeV.

11.2 Polarization

11.2.1 Polarized Muon Production

The specifications and components in the baseline design have not been optimized for polarization. Nevertheless, simple manipulations of parameters and the addition of momentum selection after phase rotation does generate significant polarization with relatively modest loss of luminosity. The only other changes required to give polarization at the interaction point are rotators in the transfer lines, and a solenoid in the collider opposite the IP.

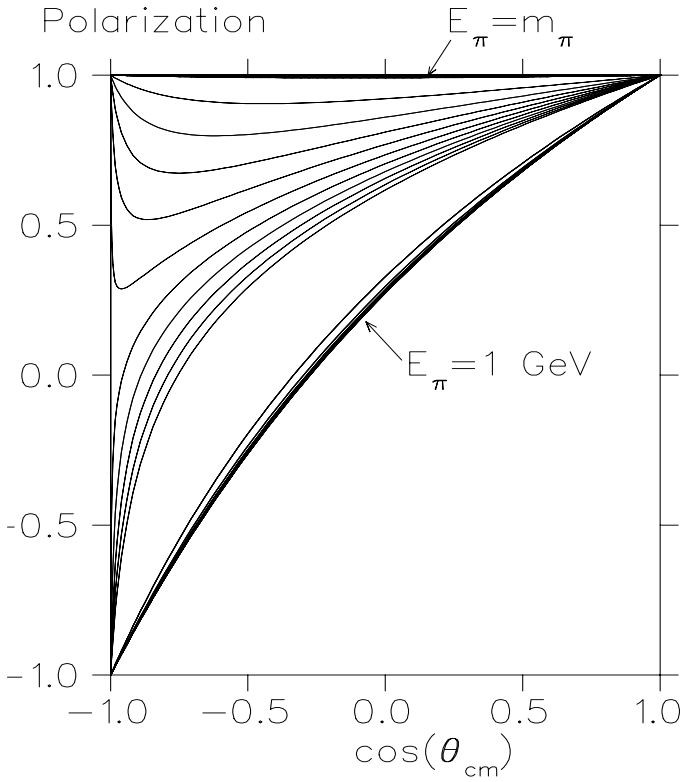

Figure 11.1: Muon polarization in the lab system vs the cosine of the center-of-mass decay angle, for a number of pion energies.

In the center of mass of a decaying pion, the outgoing muon is fully polarized (-1 for μ^+ and +1 for μ^-). In the lab system the polarization depends[1] on the decay angle θ_d and initial pion energy E_π. Fig. 11.1 shows this polarization as a function of the cosine of the center of mass decay angle, for a number of pion energies. It is seen that for pion kinetic energy larger than the pion mass, the dependence on pion energy becomes negligible. The polarization is given by $\mathcal{P} = \cos\omega$ where the Wigner angle ω satisfy the relations

$$\sin\omega = \sin\theta_{\rm cm}\frac{p_\pi^{\rm lab}}{p_\mu^{\rm lab}}\frac{m_\mu}{m_\pi} \tag{11.1}$$

$$\cos\omega = \left\{E_\pi^{\rm lab}p_\mu^{\rm cm} + \cos\theta_{\rm cm}E_\mu^{\rm cm}p_\pi^{\rm lab}\right\}/p_\pi^{\rm lab}m_\pi \tag{11.2}$$

with $p_\pi^{\rm lab}$, $E_\pi^{\rm lab}$ the pion momentum and energy in the laboratory frame and $p_\mu^{\rm lab}$, $E_\mu^{\rm cm}$ the muon momentum in the laboratory frame and energy in the center of mass. A Monte Carlo calculation[2] of the capture, decay and phase rotation gave muon polarization of approximately 0.22.

If higher polarization is required, some deliberate selection of muons from forward pion decays ($\cos\theta_d \to 1$) is required. This could be done by selecting pions within a narrow energy range and then selecting only those muons with energy close to that of the selected pions. But such a procedure would collect a very small fraction of all possible muons and would yield a very small luminosity. Instead we wish, as in the unpolarized case, to capture pions over a wide energy range, allow them to decay, and to use rf to phase rotate the resulting distribution.

Consider the distributions in velocity vs ct at the end of a decay channel. If the source bunch of protons is very short and if the pions were generated in the forward direction, then the pions, if they did not decay, would all be found on a single curved line. Muons from forward decays would have gained velocity and would lie above that line. Muons from backward decays would have lost velocity and would fall below the line. A real distribution will be diluted by the length of the proton bunch, and by differences in forward velocity due to the finite angles of particles propagating in the solenoid fields. In order to reduce the latter, it is found desirable to lower the solenoid field in the decay channel from 5 to 3 T. When this is done, and in the absence of phase rotation, one obtains the distribution shown in Fig. 11.2, where the polarization P$> \frac{1}{3}$, $-\frac{1}{3} < P < \frac{1}{3}$, and P$< -\frac{1}{3}$ is marked by the symbols '+', '.' and '-' respectively. One sees that the +'s are high, and the -'s are low, all along the distribution.

It is found that phase rotation does not remove this correlation: see Fig. 11.3. Now, after a time cut to eliminate decays from high energy pions, there is a simple correlation of polarization with the energy of the muons.

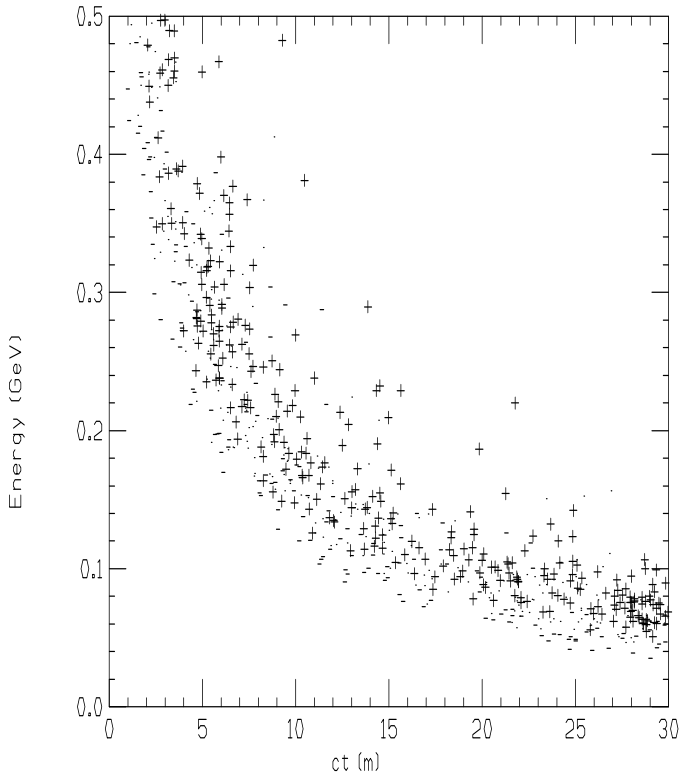

Figure 11.2: Energy vs ct of muons at end of decay channel without phase rotation; muons with polarization P$> \frac{1}{3}$, $-\frac{1}{3} < P < \frac{1}{3}$, and P$< -\frac{1}{3}$ are marked by the symbols '+', '.' and '-' respectively.

If a selection is made on the minimum energy of the muons, then for muons after the required time cut, net polarization is obtained. The higher the cut on energy, the greater the polarization, but the less the fraction $F_{loss} = N_\mu^{\rm OUT}/N_\mu^{\rm IN}$ of muons that are selected. The cut in time can probably be obtained from the phasing of the rf used to capture the bunch. Alternatively, it could be provided by a second energy cut applied after a 90 degree longitudinal phase rotation.

In order to provide the required cut on energy, one needs to generate dispersion that is significantly larger than the beam size. Collimation from one side can then select the higher energy muons. After collimation, the remaining dispersion should be removed. The generation of sufficient dispersion, in the presence of the very large emittance, is non-trivial. The only practical method appears to be the use of a bent solenoid (as discussed above in the target section). First the solenoid is bent in one direction to generate the dispersion; the collimator is introduced; then the solenoid is bend in the other direction to remove the dispersion. The complete system thus looks like an "S" or "snake".

Particles with momentum p_μ in a magnetic field B have a bending radius of R_B, given

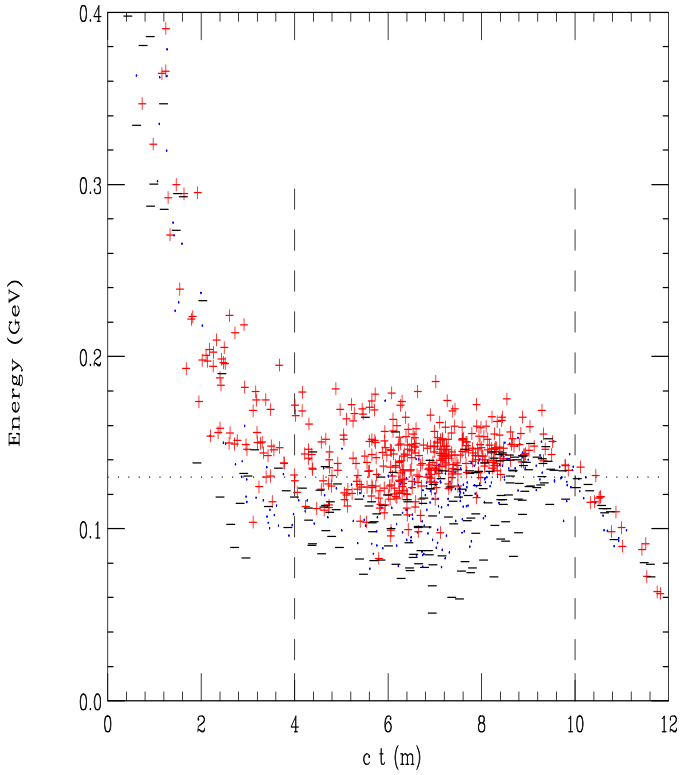

Figure 11.3: Energy vs ct of muons at end of decay channel with phase rotation; muons with polarization P$> \frac{1}{3}$, $-\frac{1}{3} < P < \frac{1}{3}$, and P$< -\frac{1}{3}$ are marked by the symbols '+', '.' and '-' respectively.

by:

$$R_B = \frac{(ep_\mu/mc)}{c\ B}. \tag{11.3}$$

If the particles are trapped in a solenoid with this field, and the solenoid is bent with a radius $R_{\rm bend}$, where

$$R_{\rm bend} >> R_B, \tag{11.4}$$

then those particles, besides their normal helical motion in the solenoid, will drift in a direction (z) perpendicular to the bend, with a drift angle ($\theta_{\rm drift} = dz/ds$) given by:

$$\theta_{\rm drift} \approx \frac{R_B}{R_{\rm bend}} \tag{11.5}$$

The integrated displacement in z, ie. the dispersion D, is then:

$$D = \theta_{drift}\ s \approx \phi\ R_B, \tag{11.6}$$

where ϕ is the total angle of solenoid bend.

As an example, we have traced typical particles with momenta of 150 and 300 MeV/c through a snake with $\phi = \pi$, $B = 1\,T$, and $R_{\rm bend} = 6\ m$. Fig. 11.4a shows the trajectories of muons as viewed from the z direction. No significant dispersion is seen. Fig. 11.4b shows the same trajectories, where the vertical positions z are plotted against s, the distance along the snake. The two momenta are seen to be dispersed during the right hand turn and recombined by the left hand turn. Negligible emittance growth is observed during the bends, but a small growth of emittance is observed at the sudden (and, in this simulation, unphysical) field gradient changes at the start and end of the bends. Even these emittance growths are acceptable providing $R_{\rm bend} > 10\ R_B$.

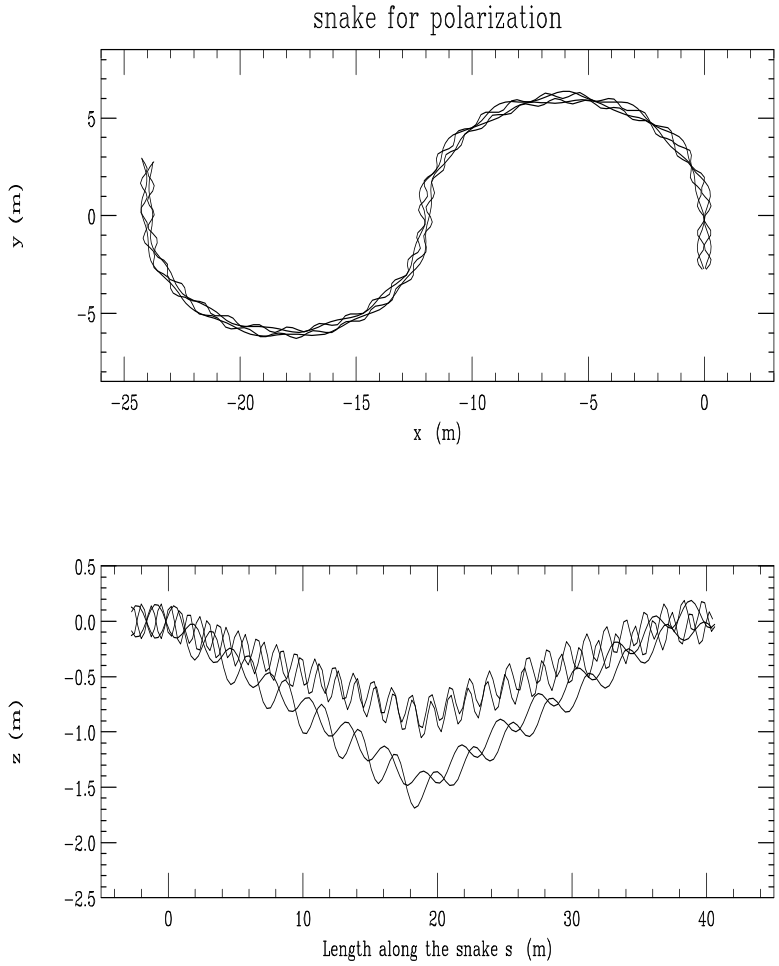

Figure 11.4: Dispersion snake: trajectories in the bending plane as seen from the perpendicular direction z (upper plot); trajectories in the vertical plane, z plotted against length along the snake s (lower plot).

Fig. 11.5 and Tb. 11.1 give the results of a Monte Carlo study in which dispersion is introduced, and progressive cuts applied, to the muons at the end of the phase rotation.

In this calculation, in order to shorten the computation time, the trajectories were not actually traced through a snake. Instead, the particles were propagated through 20 m of straight solenoid, followed by the application of dispersion equal to 6 times the momentum in GeV/c. A snake that would give such dispersion could have the parameters: solenoid field: 3 T, giving $R_B = 0.25\ m$ at the average momentum of 230 MeV/c. The diameter of the snake bends should be greater than 5 m. The bend angle required is 320 degrees, which would require some variations in bend curvature to avoid the solenoid crossing its self, but is not impractical.

Tb. 11.1 gives results for two fields in the decay channel solenoids: $5\,T$, the field in the point design; and $3\,T$, chosen to increase the polarization. It is seen that for weak cuts and small polarization, it is better to avoid the loss of muons from the lower, $3\,T$, field, but with stronger cuts the lower field gives greater polarization. In Fig. 11.5, and subsequent plots, only data from the preferred fields are shown beyond the cross over.

Table 11.1: Production polarization vs collimator position.

B (T)	cut (m)	$F_{\rm loss}$	$P_{\rm init}$	$P_{\rm final}$	$P_{\rm vec}$	$R_{v/s}$	$H_{\rm vec}$	$E_{\rm ave}$ (MeV)	δE (MeV)
5	0.00	1.000	0.23	0.18	0.36	1.45	1.03	130	23
5	1.00	0.960	0.27	0.21	0.41	1.54	1.05	144	23
5	1.12	0.890	0.30	0.24	0.46	1.64	1.06	147	20
5	1.24	0.759	0.36	0.29	0.53	1.80	1.08	151	18
5	1.30	0.614	0.41	0.33	0.60	1.99	1.11	157	17
5	1.40	0.360	0.48	0.39	0.67	2.26	1.15	166	15
5	1.50	0.163	0.56	0.45	0.75	2.64	1.20	177	15
3	0.00	0.801	0.22	0.18	0.34	1.43	1.03	130	22
3	1.06	0.735	0.29	0.23	0.44	1.61	1.05	133	22
3	1.16	0.673	0.35	0.28	0.52	1.77	1.08	137	19
3	1.26	0.568	0.41	0.33	0.59	1.98	1.11	141	17
3	1.32	0.417	0.50	0.40	0.69	2.32	1.16	147	15
3	1.40	0.264	0.59	0.47	0.77	2.78	1.22	151	13
3	1.48	0.126	0.70	0.56	0.86	3.58	1.32	159	13
3	1.56	0.055	0.77	0.62	0.90	4.25	1.38	168	12

It is seen from Tb. 11.1 that the energy cut not only increases the polarization, but also decreases the energy spread δE of the remaining muons. In Fig. 11.6 the fractional energy spread $\delta E/E$ is plotted against the loss factor $F_{\rm loss}$. The energy spread is reduced almost

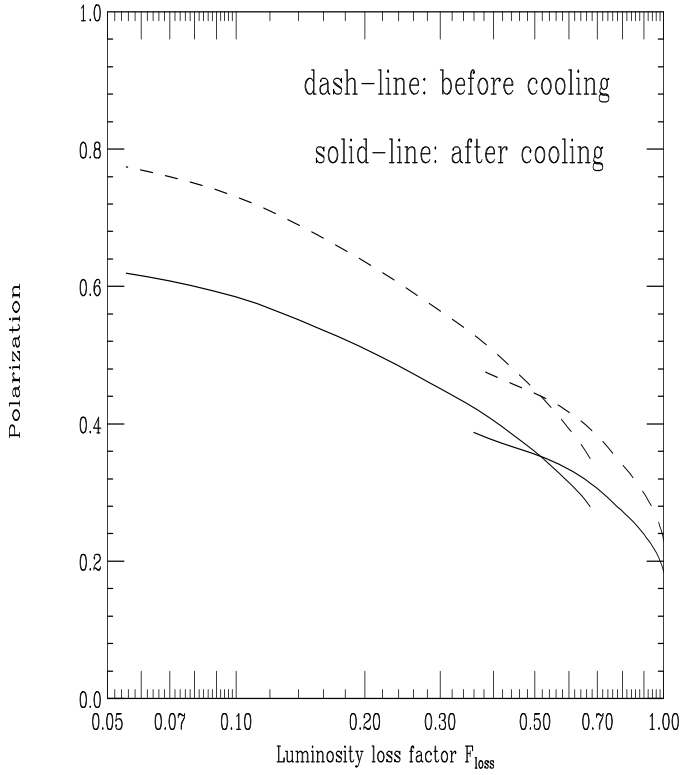

Figure 11.5: Polarization vs $F_{\rm loss}$ of muons accepted; the dashed line shows polarization as selected before cooling; the solid line gives polarization after cooling.

a factor of two for reasonable collimator positions. This reduction in energy spread would eliminate the need for the first stage of emittance cooling.

A Monte Carlo study has also been done on the effect of variations of the proton bunch length σ_t. In this study, the dispersion was not specifically introduced. Instead, polarization was generated by imposing an idealized cut on muon energies. The results of this, compared with using dispersion and a position cut, are qualitatively the same. Figure 11.7a shows the polarization before cooling as a function of σ_t for three values of the loss factor F_{loss}. It is seen that serious loss of polarization occurs when the rms width is more than 1 ns. Figure 11.7b shows the muon rms energy spread after the polarization cut. Again it is shown as a function of σ_t for three values of the loss factor F_{loss}. With no cut, the rise in energy spread would be serious ($\delta E > 20$ MeV is difficult to cool) for an rms width more than 1 ns. But with polarization cuts, the energy spread is so reduced that a larger proton bunch length would not be a problem.

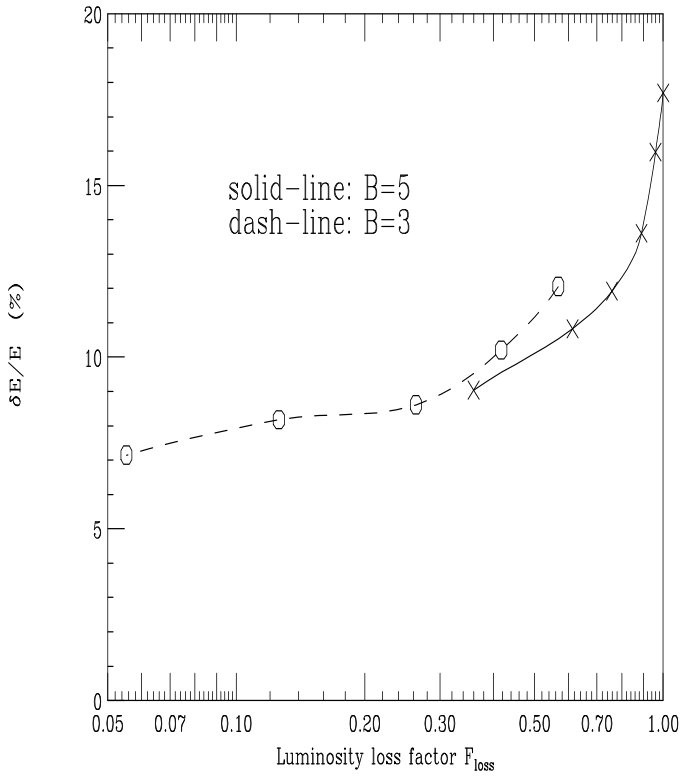

Figure 11.6: The fractional energy spread $\Delta E/E$ is plotted against the loss factor $F_{\rm loss}$ for different magnetic fields.

11.2.2 Polarization Preservation

A recent paper[3] has discussed the preservation of muon polarization in some detail. During the ionization cooling process the muons lose energy in the material and have a spin flip probability $\mathcal{P}$, where

$$\mathcal{P} \approx \int \frac{m_e}{m_\mu}\beta_v^2 \, \frac{dE}{E} \tag{11.7}$$

where β_v is the muon velocity divided by c, and dE/E is the fractional loss of energy due to ionization loss. In our case the integrated energy loss is approximately 3 GeV and the typical energy is 150 MeV, so the integrated spin flip probability is close to 10%. The change in polarization dP/P is twice the spin flip probability, so the reduction in polarization is approximately 20 %. This dilution is included in the $P_{\rm final}$ column in Tb.11.1 and is plotted as the line in Fig. 11.5.

During circulation in any ring, the muon spins, if initially longitudinal, will precess by $\gamma(g-2)/2$ turns per revolution in the ring; where $(g-2)/2$ is 1.166 10^{-3}. An energy spread $\delta\gamma/\gamma$ will introduce variations in these precession and cause dilution of the polarization. But if the particles remain in the ring for an exact integer number of synchrotron oscillations,

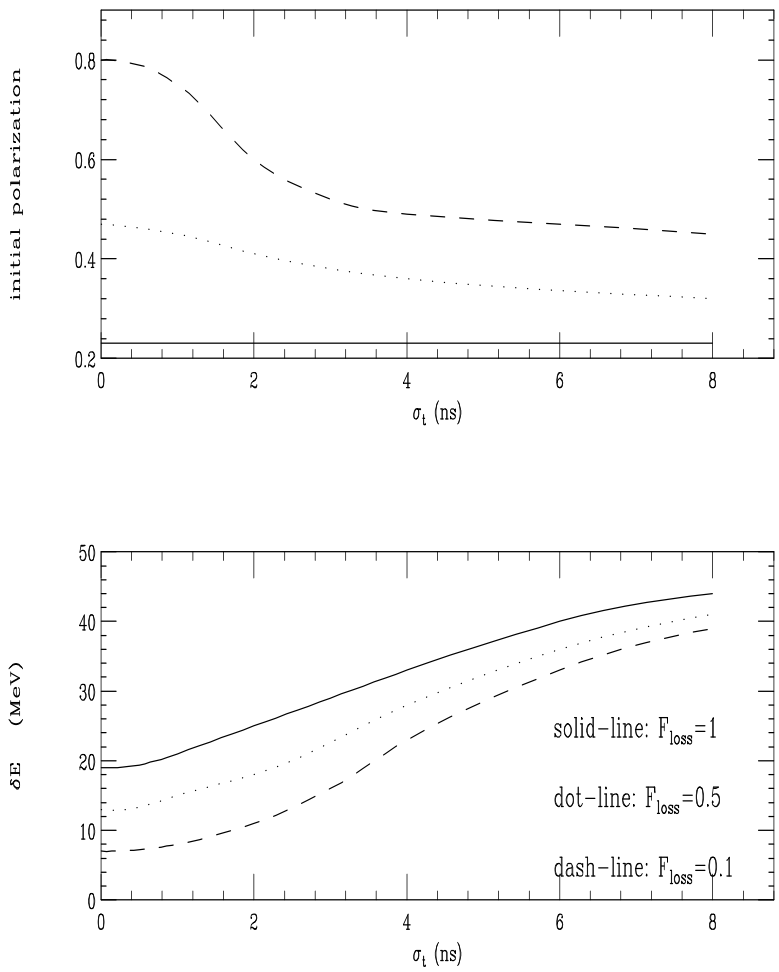

Figure 11.7: Polarization vs σ_t, the proton bunch length (upper plot). Muon *rms* energy spread vs σ_t (lower plot). Both plots for three values of the loss factor $F_{\rm loss}$.

then their individual average γ's will be the same and no dilution will occur. It appears reasonable to use this *synchrotron spin matching*[3] to avoid dilution during acceleration. In the collider, however, the synchrotron frequency will be too slow to use *synchrotron spin matching*, so one of two methods must be used:

- Bending can be performed with the spin orientation in the vertical direction, and the spin rotated into the longitudinal direction only for the interaction region. The design of such spin rotators appears relatively straightforward. The example given in the above reference would only add 120 m of additional arc length, but no design has yet been incorporated into the lattice.

- The alternative is to install a 120 m 10 T solenoid (Siberian snake) at a location exactly opposite to the intersection point. Such a solenoid reverses the sign of the horizontal

polarization and generates a cancellation of the precession in the two halves of the ring.

Provision must also be made to allow changes in the relative spins of the two opposing bunches. This could be done, prior to acceleration, by switching one of the two beams into one or the other of two alternative injection lines.

11.2.3 Benefits of Polarization of Both Beams

We consider two examples of the general advantage of having polarization in both beams. Individual physics experiments would have to be considered to determine how important such advantages are.

Consider the polarization of a vector spin state generated by the annihilation of the two muons.

$$P_{\rm vec} \;=\; \frac{F^{++} - F^{--}}{F^{++} + F^{--}} \tag{11.8}$$

When only one beam has polarization P_1, then $P_{\rm vec} = P_1$. But if both beams have polarization P in the same direction (ie. with opposite helicities), then

$$P_{\rm vec} \;=\; \frac{(P+1)^2 - (P-1)^2}{P+1)^2 + (P-1)^2} \tag{11.9}$$

In Fig. 11.8 both the polarization of each beam P, and the resulting polarization of a vector state $P_{\rm vec}$ are plotted against the loss factor F_{loss}.

A second advantage is that the ratio $R_{\rm vec/sc}$ of vector to scalar cross section can be manipulated to enhance either the vector or the scalar state. If the polarization directions have been chosen to enhance the ratio of vector to scalar states, then:

$$R_{v/s} \;=\; \frac{1+P}{1-P}. \tag{11.10}$$

Tb. 11.1 and Fig. 11.9 show this ratio as a function of the loss factor $F_{\rm loss}$.

Tb. 11.1 also shows that the fraction of total luminosity in a given state can be enhanced. If polarizations are chosen to enhance the vector state, then the fraction of vector luminosity is increased from 1/2 to $(1+P)/2$, ie. the enhancement factor $H_{\rm vec} = (1+P)$, but this is seen to be only a modest effect.

11.2.4 Luminosity Loss

If nothing else is done, then the luminosity will drop as $F^2_{\rm loss}$; where $F_{\rm loss}$ is the fraction muons lost by the muon momentum cut. At the same time, however, the space charge, wakefield, and loading during the cooling and acceleration will all be reduced; as will the beam beam

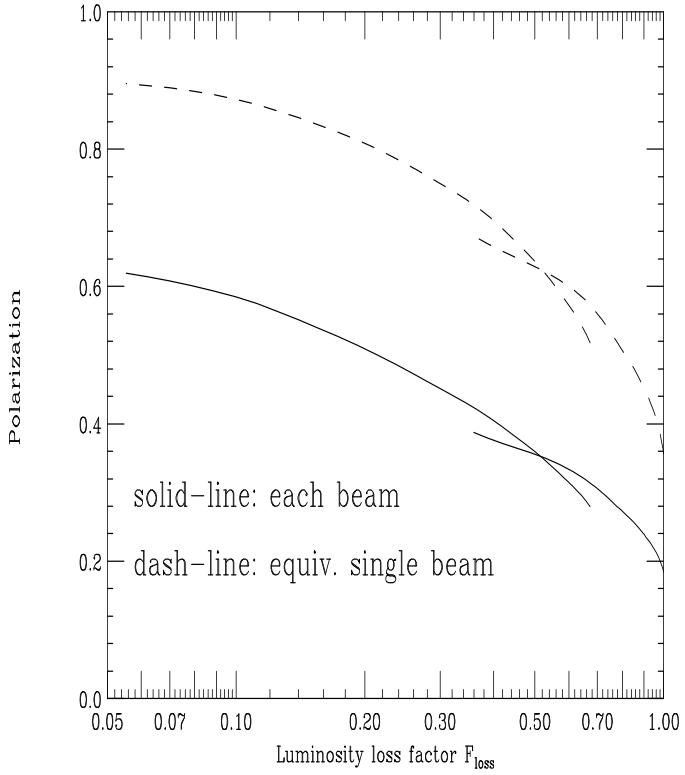

Figure 11.8: Polarization of each beam P, and the resulting polarization of a vector state $P_{\rm vec}$ vs. the loss factor $F_{\rm loss}$.

tune shift in the collider. Clearly, the cooling could now be reoptimized and some part of the lost luminosity recovered.

An alternative way to recover the luminosity would be to increase the proton bunch intensity by the factor $F_{\rm loss}$. If this were done, then the original number of muons per bunch would be generated; all the wake field, loading and space charge effects would be the same; and the luminosity per bunch crossing would be the same. If we assume that the total proton current is determined by the driver, then such an increase in proton intensity per bunch will necessitate a reduction in the number of bunches or repetition rate, by the same factor $F_{\rm loss}$. The luminosity will then fall by this factor, without the square.

For instance, in the unpolarized case of the 4 TeV collider, there were two bunches of each sign. If the momentum cut is chosen to give a value of $F_{\rm loss} = 1/2$, and the proton beam is distributed into 2 instead of 4 initial bunches, then the final number of muons per bunch, the loading, beam beam tune shift etc, would all be the same as in the unpolarized case. The luminosity would be down by a factor of only two, for polarization of 34 % in both beams.

For higher polarization at good luminosity it would be desirable to have a proton source

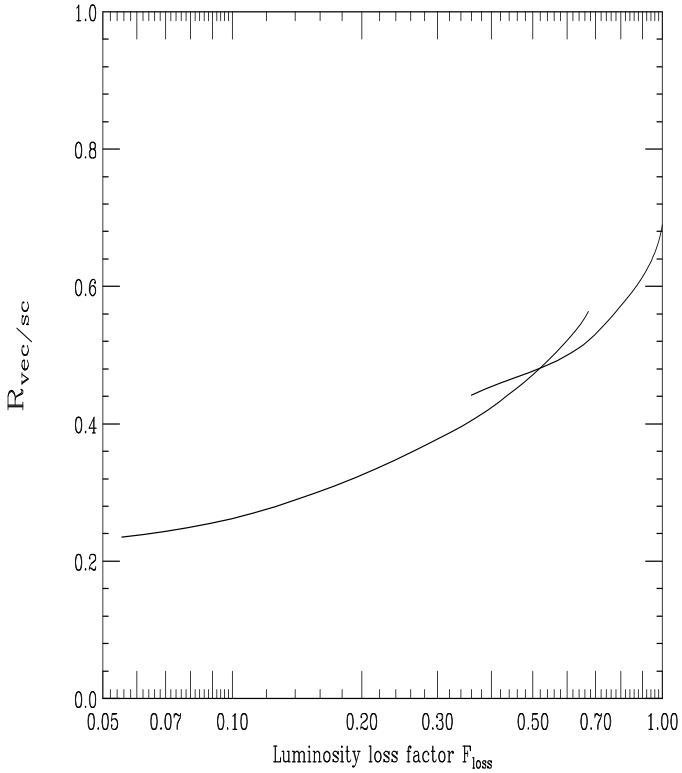

Figure 11.9: The ratio of vector to scalar states, $R_{v/s}$ vs the loss factor $F_{\rm loss}$

with the option of a lower repetition rate, but even larger numbers of protons per spill. For example 4×10^{14} protons per pulse at 4 Hz. It should then be possible to extend this method to an operation with $F_{loss} = 1/8$, and polarization of both beams of 57 %.

One also notes that the luminosity could be maintained at the full unpolarized value if the proton source intensity could be increased. Such an increase in proton source intensity in the unpolarized case would be impractical because of the resultant excessive high energy muon beam power, but this restriction does not apply if the increase is used to offset losses in generating polarization. If, for instance, the driver repetition rate were increased from 15 to 30 Hz, the fractions $F_{\rm loss}$ set at 0.5, and the number of bunches reduced to one, then the full luminosity of 10^{35} ($\rm cm^{-2}s^{-1}$) would be maintained with polarization of both beams of 34 %.

11.2.5 The Case for Polarized $\mu^+\mu^-$ Colliders

Higgs Physics

The most interesting question in particle physics now is associated with the origin of mass. It is generally assumed that the exchange of fundamental scalar particles, called the "scalar

sector" is somehow responsible for this. For super-symmetry modes, this scalar sector is even more complex and interesting (see Tb.11.2)[4]-[6].

In this section, we highlight one of the most interesting goals of a $\mu^+\mu^-$ collider: the discovery of a Higgs boson in the mass range beyond that to be covered by LEP I & II ($\sim$ 80–90 GeV) and the natural range of the supercolliders.

With a high-mass t quark, precision LEP/SLD data and the theorists' dreams of a SUSY world, the scalar (pseudoscalar sector) is possibly very complex and may require several types of colliders[7]. Consider:

- If the low-mass Higgs has $m > 130$ GeV, MSSM is not allowed.
- If $m > 200$ GeV, there are constraints from the requirement that perturbation theory be useful up to very high energy and from the stability of the vacuum.
- If $m < 130$ GeV, MSSM is possibly allright, but we may expect other particles (H, A) and the width of the low mass Higgs may change.
- The scalar sector may be extremely complex, requiring pp (LHC) and $\mu^+\mu^-$ colliders (and possibly NLC and $\gamma\gamma$ colliders).
- In high energy collisions, vector states are allowed unless a special method is used. Consider $\mu^+\mu^-$ colliders with polarized $\mu^\pm$

Table 11.2: The scalar sector

	(100–500) GeV	scalars $(H, A, ...)$
	$\nearrow$	
$\mu^+\mu^-$		
	$\searrow$	
	≥ 2 TeV	W^+W^-
		Z^0Z^0 production in scalars

This cannot be done for pp or e^+e^- colliders.

- A $\mu^+\mu^-$ collider is complimentary to the LHC/CMS detector.

There are several ways to determine the approximate mass of the Higgs boson in the future[7]. Suppose it is expected to be at a mass of 135 $\pm$ 2 GeV, the energy spread of a

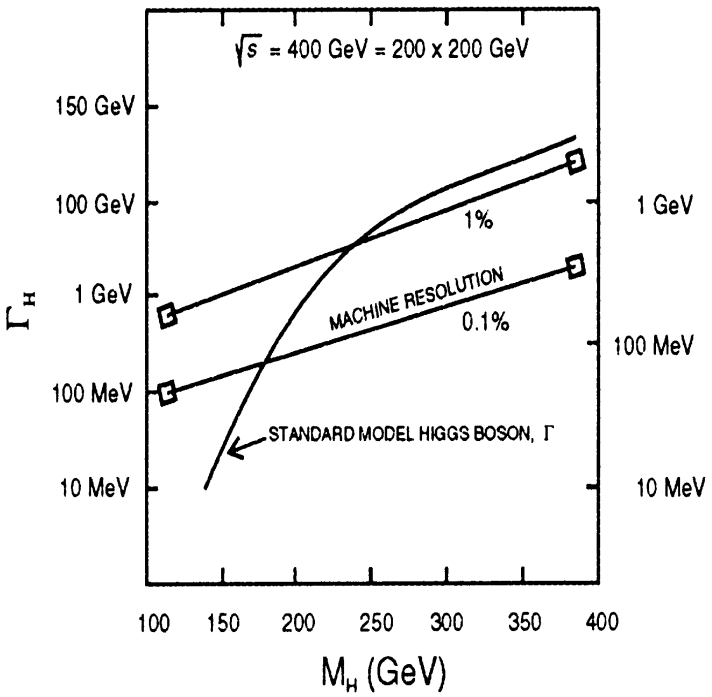

Figure 11.10: Higgs search at a $\mu^+\mu^-$ collider (required machine resolution and the expected Higgs width).

$\mu^+\mu^-$ collider can be matched to the expected width (see Fig.11.10). An energy scan could yield a strong signal to background especially with polarized $\mu^+\mu^-$ in the scalar configuration [5],[7]. Once the Higgs is found, the following could be carried out:

1. Measurement of width, to separate Standard Model Higgs from SUSY or other Higgs models[5],

2. Measurement of the Branching fractions, the rare decay will involve loop effects that can sample very high energies.

Polarization will play an essential role for any $\mu^+\mu^-$ collider [5],[6]

Production of Polarized $\mu^\pm$ Beams

Polarization is natural for $\mu^\pm$, since they are produced in weak decays and are initially fully polarized because of the V–A interaction. There are three proposed methods for producing intense polarized $\mu^\pm$ beams:

- Accelerate polarization and cool the $\pi^\pm$ (A. Skrinsky *et al.*)[8]

Table 11.3: Depolarization processes in the $\mu^+\mu^-$ complex (Norum Rossmanith scheme)

	Plan	Comments
1.	Decay channel (some acceleration also)	Use synchrotron spin matching; Small effect on polarization.
2.	Cooling channel ($P \sim P_0\ e^{(-K/a)}$, where $a \sim 200$ m for Be).	Depolarization $\sim (m_e/m_\mu)\beta^2$; For $\beta \sim 0$, the effect is very small.
3.	During acceleration to 250 GeV or 2 TeV (CEBAF-type recirculation does not cause severe depolarization)	Cross integer resonances (3 for 250GeV, 21 for 2 TeV); Two effects cause depolarization during acceleration: energy spread and resonances.
4.	Depolarization in collider	Possible large depolarization; spin rotation will be needed to keep small

- Use $K^\pm$ decays and "narrow-band neutrino-like beam" (D. Cline)
- Use pion decays and a short proton bunch (R. Palmer *et al.*)[9].

Fig.11.5 shows the tradeoff between intensity and polarization in one of these schemes[9]. This is one of the major areas of research for $\mu^+\mu^-$ colliders.

Polarization Preservation in the $\mu^+\mu^-$ Collider Complex

R. Rossmanith[3] has presented a scheme to ensure polarization preservation. Because of the value of the $(g-2)_\mu$ for the $\mu^\pm$, it should be much easier to maintain large polarization provided certain steps are taken in the collider complex[3]. The preferred polarization state up to the high energy collider will be longitudinal. These steps are outlined here in Tb.11.3 and in Fig.11.11[3]. It is extremely good news that a $\mu^+\mu^-$ collider with high polarization may be feasible, provided the initial problem of achieving high polarization at the source is solved. This is one of the major problems of a $\mu^+\mu^-$ collider.

In Fig.11.11a it is shown a possible scenario for arranging the spin rotators in order to obtain varying helicity directions from interaction to interaction. After the particles have passed the two spin rotators surrounding the interaction region, the spin aims in the opposite direction and changes its direction the next time it passes the interaction region. This means that polarized interactions with a low systematic error can be obtained. In Fig.11.11b it is

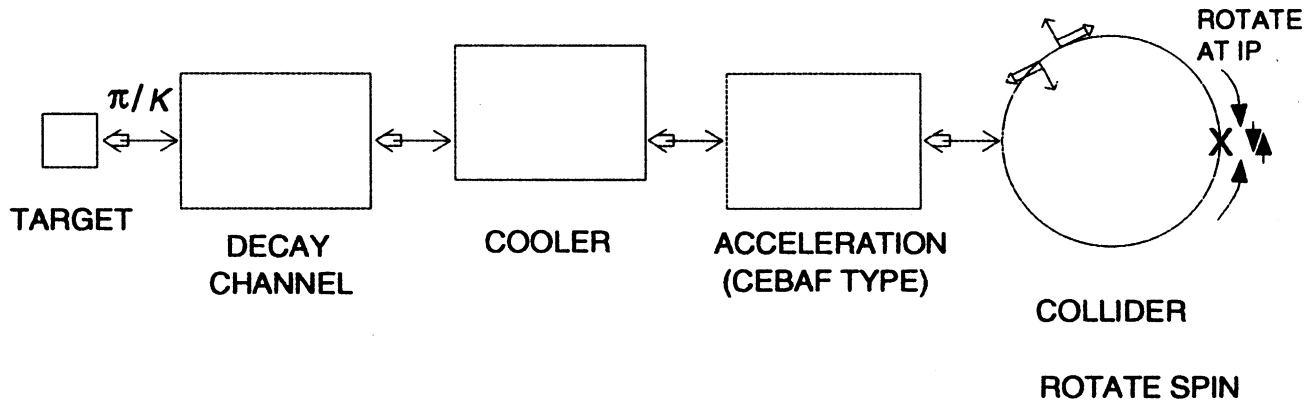

Figure 11.11: (A) A possible scenario for arranging the spin rotators; (B) Possible spin rotator for muons in the main ring

shown a possible spin rotator for the main ring. The spins are rotated 45 degrees from the vertical towards the momentum axis by the first three ca. 10-T, 10-m-long vertically deflecting magnets. The spin is afterwards rotated by 180 degrees around the vertical axis by 12 normal bending magnets and finally into the longitudinal direction by the last three vertically deflecting magnets. The additional space requirement for the spin rotators is 120 m on each side of the interaction region. H and V denote, respectively, horizontally and vertically deflecting magnets

t Quark Physics

The status of the t quark study from FNAL for the CDF detector was reviewed by D. Amidei[10]. In Fig.11.12, we show that Feynman diagrams for the production of $t\bar{t}$ for both e^+e^- and $\mu^+\mu^-$ collisions[6]. Because of the larger mass of the μ compared to the e, the diagram with a scalar intermediate state can be important (see process depicted in Fig.11.12b). If we fully polarize the $\mu^+\mu^-$ system to give a net zero scalar state, we believe the scalar sector will be enhanced to the point that a measurable asymmetry will be generated. Thus, one could search for evidence of a scalar particles far from the central mass. This is a unique feature of polarized $\mu^+\mu^-$ colliders[6]. The detector design will play a crucial role in such studies[11],[12].

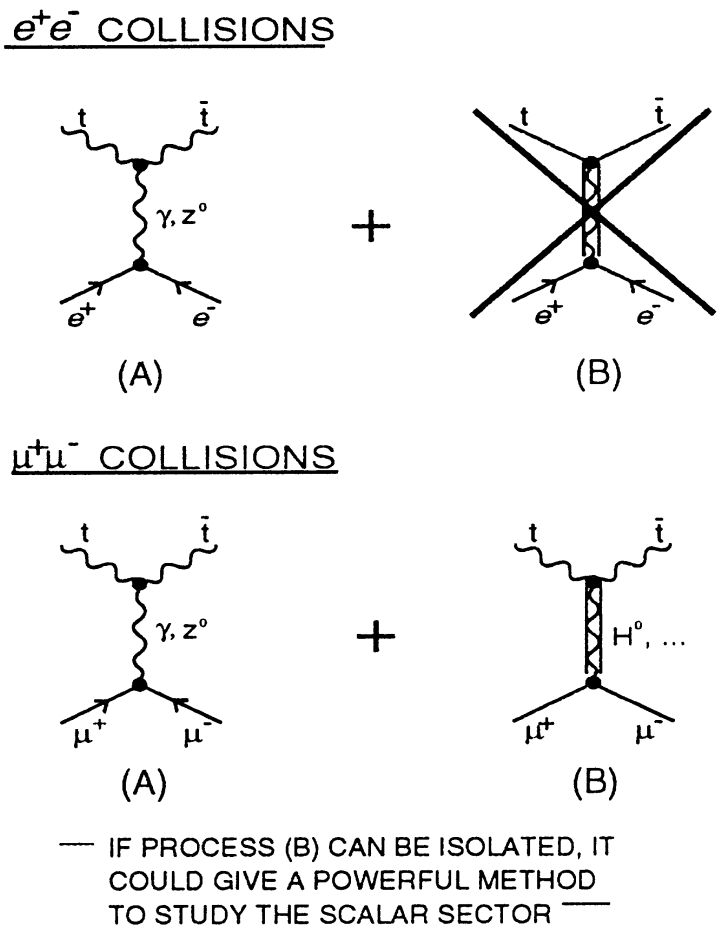

Figure 11.12: $t\bar{t}$ production at $\mu^+\mu^-$ colliders.

11.3 Scaling of Luminosity vs Energy and Momentum Spread

The bunch populations decay exponentially, yielding an integrated luminosity equal to its initial value multiplied by an *effective* number of turns $n_{\rm eff} = 150\ B$, where B is the mean bending field in T.

The luminosity is given by:

$$\mathcal{L} \;=\; \frac{\mathrm{N}_\mu^2\ \mathrm{f_{rep}}\ \mathrm{n_{eff}} \mathrm{n_b} \gamma}{4\pi\ \beta^*\ \epsilon_\mathrm{n}} \mathrm{H(A,D)} \tag{11.11}$$

where N_μ is the number of muons in one bunch, n_b is the number of bunches and the enhancement factor $H(A,D)$ is[13]

$$H(A,D) \approx 1 + D^{1/4}\left[\frac{D^3}{1+D^3}\right]\left\{\ln\left(\sqrt{D}+1\right) + 2\ln\left(\frac{0.8}{A}\right)\right\}, \tag{11.12}$$

with $A = \sigma_z/\beta^*$, and $D = \frac{\sigma_z n_\mu}{\gamma \sigma_t^2} r_e(\frac{m_e}{m_\mu})$.

In the cases we are considering: $A \approx 1$, $D \approx 0.5$ and $H(A, D) \approx 1$.

11.3.1 Luminosity vs Energy, for a Given Ring

For a fixed collider lattice, operating at energies lower than the design value, the luminosity will fall as γ^3. One power comes from the γ in Eq.11.11; a second comes from n_e, the effective number of turns, that is proportional to γ; the third factor comes from β^*, which must be increased proportional to γ in order to keep the beam size constant within the focusing magnets. The bunch length σ_z must also be increased proportional to γ so that the required longitudinal phase space is not decreased; so A $= \sigma_z/\beta^*$ remains constant.

11.3.2 Scaling for Collider Rings for Different Energies

As noted above, the luminosity in a given ring will fall as the third power of the energy at which it is operated. Such a drop is more rapid than the gain in typical cross sections, and, as we shall see, it is more rapid than the drop in luminosity obtained with rings designed for the lower energies. It would thus be reasonable, having invested in a muon source and accelerator, to build a sequence of collider rings at spacings of factors of 2-3 in maximum energy. We will now derive scaling rules for such collider rings.

The luminosity

$$\mathcal{L} \;=\; \frac{N_\mu^2 \; n_{eff} n_b f_{rep} \; \gamma}{4 \; \pi \; \epsilon_n \; \beta^*} \;\propto\; \frac{N_\mu \; I_\mu \; \gamma}{\epsilon_n \; \beta^*} \tag{11.13}$$

which, since $\Delta\nu_{bb}$, the beam beam tune shift is given by:

$$\Delta\nu_{bb} \;\propto\; \frac{N_\mu}{\epsilon_n}, \tag{11.14}$$

gives:

$$\mathcal{L} \;\propto\; \frac{I_\mu \; \Delta\nu_{bb} \; \gamma}{\beta^*} \tag{11.15}$$

where $I_\mu = N_\mu n_b f_{rep}$ is the muon flux.

If a final focus multiplet is scaled keeping the relative component lengths and the pole tip fields constant, then one obtains:

$$\ell^* \;\propto\; \sqrt{a_{max} \; \gamma} \tag{11.16}$$

$$\theta^* \;\propto\; \sqrt{\frac{a_{max}}{\gamma}} \propto \sqrt{\frac{\epsilon_n}{\beta^* \; \gamma}} \tag{11.17}$$

$$\beta^* \;\propto\; \frac{\epsilon_n}{a_{max}} \tag{11.18}$$

where θ^* is the rms angle of muons diverging from the focus. ℓ^* is the free space from the target to the first quadrupole (proportional to all quadrupole lengths in the multiplet), and a_{max} is the maximum aperture of any quadrupole (proportional to all apertures in the multiplet).

The normalized emittance ϵ_n is constrained by the ionization cooling, but since one can exchange transverse and longitudinal emittance, it is, in principle, the six dimensional emittance ϵ_6 that is constrained. Extending the lepton emittance conventions, we define:

$$\epsilon_6 \;=\; (\epsilon_n)^2 \; \delta\sigma_z\gamma\beta_v. \tag{11.19}$$

where $\delta = \frac{\delta p}{p}$. With this definition, the area of the six dimensional phase space is given by, $\Phi_6 \;=\; \pi^3 \; m_\mu^3 \; \epsilon_6$. σ_z cannot be large compared with the focus parameter β^*, so, taking them to be proportional to one another, and taking the normalized velocity $\beta_v = 1$, then:

$$\epsilon_6 \;\propto\; (\epsilon_n)^2 \; \delta\beta^*\gamma \tag{11.20}$$

and from the above:

$$(\epsilon_n)^3 \;\propto\; \frac{\epsilon_6 \; a_{max}}{\gamma \; \frac{dp}{p}} \tag{11.21}$$

$$(\beta^*)^3 \;\propto \frac{\epsilon_6}{\gamma \; \delta \; a_{max}^2} \tag{11.22}$$

11.3.3 Six Dimensional Emittance Dependence on N_μ and ϵ_n

The six dimensional emittance ϵ_6 obtained from the cooling will, because of more detailed constraints, depend to some extent on the number of muons n_μ, and on the final transverse emittance ϵ_n.

The dependence on the number of muons is relatively straightforward. As the number of muons per bunch rises, the longitudinal space charge forces increase and it becomes impossible, without changing the rf systems, to maintain the same bunch lengths. As a result the bunch lengths must be increased by the square root of the number of muons.

A study, using the analytic formulae, was used to derive cooling sequences with differing parameters. First, sequences were calculated with numbers of initial muons per bunch of 1, 2, 3.75, 7.5, and 15 x 10^{12} (corresponding to muons in the collider of .1, .2, 1, 2, and 4 x 10^{12}). The final transverse emittance at the end of the cooling was required to be 4 10^{-5} m, (corresponding to an emittance in the collider of 5 10^{-5} m). The six dimensional emittances obtained are plotted in Fig. 11.13a. It is seen that for $N_\mu > 10^{12}$ the six dimensional emittances are indeed approximately proportional to the root of the number of muons (the line shows this dependence).

The study also obtained cooling sequences giving six dimensional emittances for a range of final transverse emittances. The dependence here is more complicated. If emittance exchange between longitudinal and transverse emittances could be achieved without material then the six dimensional emittance should be independent of the final transverse emittance chosen. But the exchange does require material wedges, and Coulomb scattering in those wedges increases the six dimensional emittances; and it does so to a greater extent if the transverse emittance is small. In Fig. 11.13b, we show the six dimensional emittances obtained for 5 representative transverse emittances. Over the range of interest the dependence of ϵ_6 is approximately the inverse root of ϵ_n (the line shows this dependence).

For the purposes of this study, we may thus assume that:

$$\epsilon_6 \ \propto \ \sqrt{\frac{N_\mu}{\epsilon_n}} \tag{11.23}$$

11.3.4 Energy Scaling, Allowing the Emittances to Vary

If N_μ is limited by the beam beam tune shift:

$$N_\mu \ \propto \ \epsilon_n \ \Delta\nu_{bb} \tag{11.24}$$

substituting this in equation 11.23:

$$\epsilon_6 \ \propto \ \sqrt{\Delta\nu_{bb}} \tag{11.25}$$

giving:

$$\epsilon_n \ \propto \ \Delta\nu_{bb}^{1/6} \ \left(\frac{a_{\max}}{\gamma \ \delta}\right)^{1/3} \tag{11.26}$$

$$\beta \ \propto \ \frac{\epsilon_n}{a_{\max}} \tag{11.27}$$

$$n_\mu \ \propto \ (\Delta\nu_{bb})^{1\frac{1}{6}} \ \left(\frac{a_{\max}}{\gamma \ \delta}\right)^{1/3} \tag{11.28}$$

$$\tag{11.29}$$

so:

$$\mathcal{L}|_{\Delta\nu} \ \propto \ I_\mu \ \gamma^{4/3} \ \Delta\nu_{bb}^{5/6} \ a_{\max}^{2/3} \ (\delta)^{1/3} \tag{11.30}$$

One notes however that as γ or δ decreases the required number of muons N_μ rises, and will at some point become unreasonable. If we impose a maximum number of muons $N_{\max}$, then, when this bound is reached,

$$\epsilon_n \propto \ N_{\max}^{1/7} \ \left(\frac{a_{\max}}{\gamma \ \delta}\right)^{2/7} \tag{11.31}$$

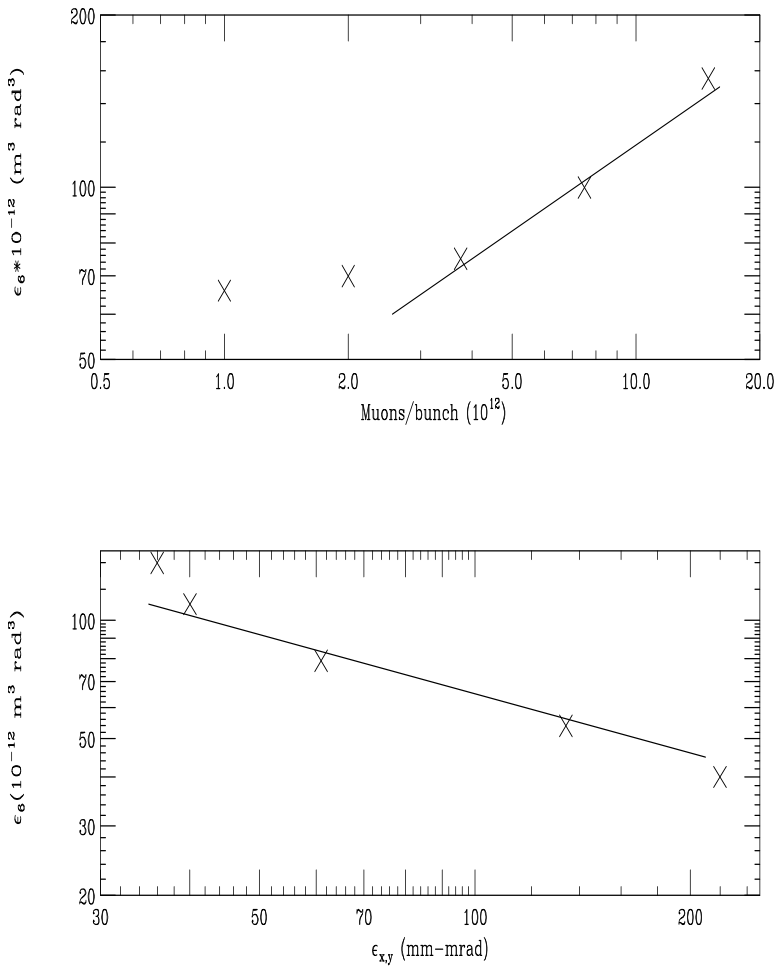

Figure 11.13: Six-dimensional emittance ϵ_6 vs a) muon intensity N_μ entering the cooling section; b) the transverse emittance ϵ_n at the end of the cooling section.

$$\beta \propto \frac{\epsilon_n}{a_{\max}} \tag{11.32}$$

and:

$$\mathcal{L}|_{N_\mu} \propto I_\mu N_{\max}^{12/7} \gamma^{11/7} a_{\max}^{3/7} \left(\frac{\delta p}{p}\right)^{4/7} \tag{11.33}$$

Using the above relationships. and assuming a constant value of $a_{\max}$ we obtain the scaled parameters for a sequence of colliding rings given in Tb. 11.4. Fig.11.14 shows the luminosities that would be available at all energies, including those requiring the use of rings at energies less than their maximum. The lines and dashed lines indicate the luminosities with a bound on N_μ of 4 10^{12}. The line gives luminosities for the nominal rms $\delta p/p$ of 0.12 %, while the dashed line is for a $\delta p/p$ of 0.01 %.

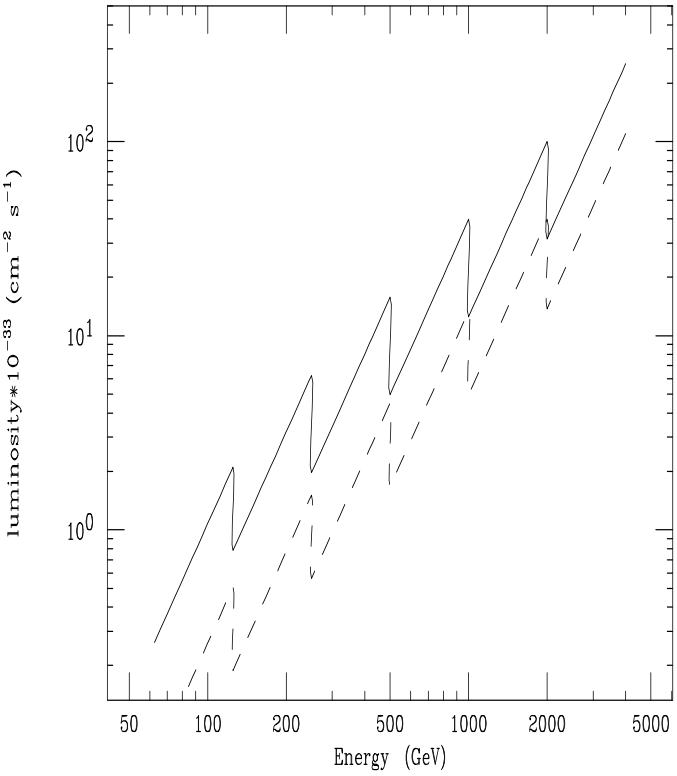

Figure 11.14: Luminosity vs energy assuming rings spaced by factors of two in energy; the line is for $\delta E/E = 0.12\,\%$, the dashed line is for $\delta E/E = 0.01\,\%$.

Table 11.4: Scaling of parameters with energy and momentum spread

E (GeV)	Luminosity ($cm^{-2}s^{-1}$)	emittance (m-rad)	$\#\mu$ (10^{12})	$\delta\nu$	β (mm)	len* (m)	$\beta_{\max}$ (km)	chrom	$\delta E/E$ (%)
4000	2.5E+35	4.0E-05	1.6	0.040	2.4	9.2	882	12829	0.12
2000	1.0E+35	5.0E-05	2.0	0.040	3.0	6.5	350	3600	0.12
1000	4.0E+34	6.3E-05	2.5	0.040	3.8	4.6	139	1010	0.12
500	1.6E+34	7.9E-05	3.2	0.040	4.8	3.3	55	283	0.12
250	6.3E+33	1.0E-04	4.0	0.040	6.0	2.3	22	80	0.12
125	2.1E+33	1.2E-04	4.0	0.033	7.3	1.6	9	23	0.12
4000	1.1E+35	9.1E-05	3.6	0.040	5.5	9.2	385	5604	0.01
2000	4.0E+34	1.1E-04	4.0	0.036	6.7	6.5	156	1603	0.01
1000	1.3E+34	1.4E-04	4.0	0.029	8.2	4.6	64	465	0.01
500	4.5E+33	1.7E-04	4.0	0.024	10.0	3.3	26	135	0.01
250	1.5E+33	2.0E-04	4.0	0.020	12.2	2.3	11	39	0.01
125	5.1E+32	2.5E-04	4.0	0.016	14.9	1.6	4	11	0.01

Bibliography

[1] K. Assamagan, et al., Phys Lett. **B**335, 231 (1994); E. P. Wigner, Ann. Math. **40**, 194 (1939) and Rev. Mod. Phys., **29**, 255 (1957).

[2] R. Palmer et al., *Muon Collider Design*, *Proceedings of the Symposium on Physics Potential and Development of* $\mu^+\mu^-$ *Colliders*, San Francisco, CA (1995); Supplement to Nuclear Physics B, to be published.

[3] B. Norum and R. Rossmanith, *Polarized Beams in a Muon Collider*, *Proceedings of the Symposium on Physics Potential and Development of* $\mu^+\mu^-$ *Colliders*, San Francisco, CA (1995); Supplement to Nuclear Physics B, to be published.

[4] D. Cline, Nucl. Instrum./Meth., A 350 (1994) 24, and the following four papers (pp. 27-56), which constitute a mini-conf. proceeding of the Napa meeting.

[5] V. Barger *et al.*, "Particle Physics Opportunities at $\mu^+\mu^-$ Colliders," in *Physics Potential & Development of* $\mu^+\mu^-$ *Colliders* (Proc., 3rd Int. Conf., San Francisco, Dec. 1995), Elsevier, in press.

[6] D. B. Cline, "Physics Potential of Polarized $\mu^+\mu^-$ Colliders," to be published in the Proceedings of the Montauk Workshop on $\mu^+\mu^-$ Colliders, Nov. 1995.

[7] D. Cline, "Physics Potential and Development of $\mu^+\mu^-$ Colliders," UCLA preprint CAA-115-12/94 (1994).

[8] A. Skrinsky, "Polarized Muon Beams for a Muon Collider," in *Physics Potential & Development of* $\mu^+\mu^-$ *Colliders* (Proc., 3rd Int. Conf., San Francisco, Dec. 1995), Elsevier, in press.

[9] R. Palmer *et al.*, "Muon Collider Design," in *Physics Potential & Development of* $\mu^+\mu^-$ *Colliders* (Proc., 3rd Int. Conf., San Francisco, Dec. 1995), Elsevier, in press.

[10] D. Amidei, "Top Physics at the Fermilab Tevatron," in *Physics Potential & Development of $\mu^+\mu^-$ Colliders* (Proc., 3rd Int. Conf., San Francisco, Dec. 1995), Elsevier, in press.

[11] M. Atac, "Detector Possibilities for a $\mu^+\mu^-$ Collider in *Physics Potential & Development of $\mu^+\mu^-$ Colliders* (Proc., 3rd Int. Conf., San Francisco, Dec. 1995), Elsevier, in press.

[12] V. Polychronakos, "$\mu^+\mu^-$ Detector Studies," in *Physics Potential & Development of $\mu^+\mu^-$ Colliders* (Proc., 3rd Int. Conf., San Francisco, Dec. 1995), Elsevier, in press.

[13] P. Chen and K. Yokoya, Phys. Rev. **D38** 987 (1988); P. Chen, *SLAC-PUB-4823* (1987); Proc. Part. Accel. School, Batavia, IL, (1987); AIP Conf. Proc. **184**, 633 (1987).

Contributors

- R. B. Palmer, (BNL/SLAC) Editor
- D. Cline, (UC, Los Angeles)
- R. Rossmanith, (DESY)
- B. Norum, (Univ. Virginia)

List of Figures

List of Tables